GIWA, A., SHEHU, H., RAMALAN, M., ORAKWE, I., ABUNOMAH, O., OGUNLUDE, P., WILLIAMWEST, T., IGBAGARA, W., OGOUN, E., HASHIM, I., AISUENI, F. and GOBINA, E. 2022. Microporous alumina–silica composite membrane with very low N2 permeability but high CO2 selectivity for direct air capture. In Khan, A.A., Ciddi, M.L. and Unal, M. (eds.) *Proceedings of the 2022 International conference on studies in engineering, science and technology (ICSEST 2022)*, 10-13 November 2022, Antalya, Turkey. Ames, IA: International Society for Technology, Education and Science (ISTES) [online], pages 182-210. Available from: https://www.istes.org/seeder/books/files/54c86815762a9dac0440e35d04a1e05c.pdf

Microporous alumina–silica composite membrane with very low N2 permeability but high CO2 selectivity for direct air capture.

GIWA, A., SHEHU, H., RAMALAN, M., ORAKWE, I., ABUNOMAH, O., OGUNLUDE, P., WILLIAMWEST, T., IGBAGARA, W., OGOUN, E., HASHIM, I., AISUENI, F. and GOBINA, E.

2022

Microporous Alumina–Silica Composite Membrane with Very Low N_2 Permeability but High CO_2 Selectivity Considered for Direct Air Capture

Ayo Giwa

McAlpha, Inc., 205 - 279 Midpark Way SE, Calgary, Alberta T2X 1M2, Canada

Habiba Shehu, Muktar Ramalan, Ifeyinwa Orakwe, Ofasa Abunomah, Priscilla Ogunlude, Tamunotonye Williamwest, Woyintonye Igbagara, Evans Ogoun, Idris Hashim, Florence Aisueni and Edward Gobina*

Centre of Excellence for Process Integration and Membrane Technology (CPIMT), School of Engineering, Robert Gordon University, Garthdee Road, Aberdeen, AB10 7GJ, UK

Abstract: This research involves technical approaches to capture carbon dioxide (CO_2) from ambient air involving a filter with a transport mechanism described based on experimental results. A silica inorganic composite membrane was prepared by using a silicone elastomer precursor using the sol-gel method on the 15 nm pore of a TiO_2/gamma alumina support commercially available. All experiments were single gas transport. CO_2, nitrogen (N_2) and methane (CH_4) flowrates were measured through the support, 1st dip coated and 2nd dip coated membranes respectively at room temperature and transmembrane pressure drops ranging from 0.01 to 0.1 bar. N_2 was completely blocked from going through the CO_2 membrane following the 2nd dip coating. The permeance of CO_2 in this membrane is much lower than that in only pure silica, and it is thought to possess two types of micropores, ultra-micropores through which only very small molecules such as helium (He) and hydrogen (H_2) can permeate through and a rather small number of micropores in which molecules such as CO_2 and N_2 were able to flow through but not simultaneously as they are unable to pass one another within the pores due to selective adsorption of CO_2. At low transmembrane pressure drop the membranes showed complete blockage of N_2 and only CO_2 was able to permeate over the transmembrane pressure drop of 0.01-0.04 bars. This significant because in DAC renewable energy can be used to power fans/blowers that force the air through the membranes thus making the specific energy requirement lower than that of the adsorption and absorption processes, together with higher productivity levels.

Keywords: Carbon dioxide, Direct Air Capture, Ambient Air, Membrane, Silica, Ceramic

Citation: Giwa, A., Shehu, H., Ramalan, M., Orakwe, I., Abunomah, O., Ogunlude, P., Williamwest, T., Igbagara, W., Ogoun, E., Hashim, I., Aisueni, F., & Gobina, E. (2022). Microporous Alumina–Silica Composite Membrane with Very Low N_2 Permeability but High CO_2 Selectivity Considered for Direct Air Capture. In A. A. Khan, M. L. Ciddi, & M. Unal (Eds.), *Proceedings of ICSEST 2022-- International Conference on Studies in Engineering, Science, and Technology* (pp. 182-210), Antalya, Turkiye. ISTES Organization.

Introduction

One of the key takeaways from COP26 in Glasgow, UK between 31 October to 12 November was the urgent decarbonization required to meet the Paris Agreement target of 1.5°C warming. In the COP27 held in the resort town of Sharm el-Sheikh, Egypt, from 7-18 November 2022 leaders were under pressure to start delivering on the promises made in the 2021 Glasgow Climate Pact. Russia's war against Ukraine has resurrected deep fault lines in international relations not seen since after the Cold War, while sanctions on Russian oil and gas have created a rush to exploit more fossil fuels and demand spikes making energy security a priority and putting climate change policy in the background.

Nevertheless, recent climatic events ranging from record floods in Nigeria and Pakistan to record droughts in China and parts of Europe exacerbated by heat waves continue to remind the world that climate change is real, and the problem is worsening. The global average atmospheric carbon dioxide (CO_2) concentration set another record high when it peaked in May 2022 at 421 parts per million. Prior to the Industrial Revolution, CO_2 levels were consistently around 280 ppm for almost 6,000 years of human civilization (Watson, S. K., June 7, 2022). Reducing CO_2 emissions alone will not suppress global warming, and it is necessary to capture the CO_2 from hard to abate sectors such as aviation and shipping and that which has been cumulatively emitted into the atmosphere over the years as well.

For this reason, negative CO_2 emission technology, a technology capable of removing CO_2 from the atmosphere, is considered essential. More especially, direct capture of CO_2 from the air, so-called direct air capture (DAC) (Figure 1) has attracted much attention in recent years as one of promising negative technologies, because of the high potential capacity of CO_2 capture. One area where the impact of negative emissions can make a significant impact is in aviation which has been under increasing pressure from both consumers and scientists to try to find proper ways to decarbonise air travel for several years, albeit with limited success.

More recently, however, at the International Civil Aviation Organisation (ICAO), triennial assembly in Montreal, Canada, on the 7th of September2022 member states finally agreed to support a net zero target for 2050. This development will significantly increase demand for DAC technologies in the next three decades to 2050. In general, absorption, adsorption, and membrane separation are known as representative CO_2 capture technologies, and DAC is essentially based on these technologies.

DAC systems using absorption and adsorption methods have already reached the level of plant scale, with several plants in operation and many more planned but the desorption process of the captured CO_2 from the absorbent or adsorbent requires heating to recover the captured CO_2 which consumes a large amount of energy and water.

On the other hand, membrane separation is generally considered as a most cost- and energy-efficient process among these capture technologies, but DAC by membrane separation has not been considered at all due to the immaturity of the membrane performance for low CO_2 concentration capture, especially CO_2 permeance. However, recent developments in the learning of membrane technology and significant cost-reduction in renewable energy production has brought the possibility that membrane processes can be considered as a new approach to DAC (Figure 1).

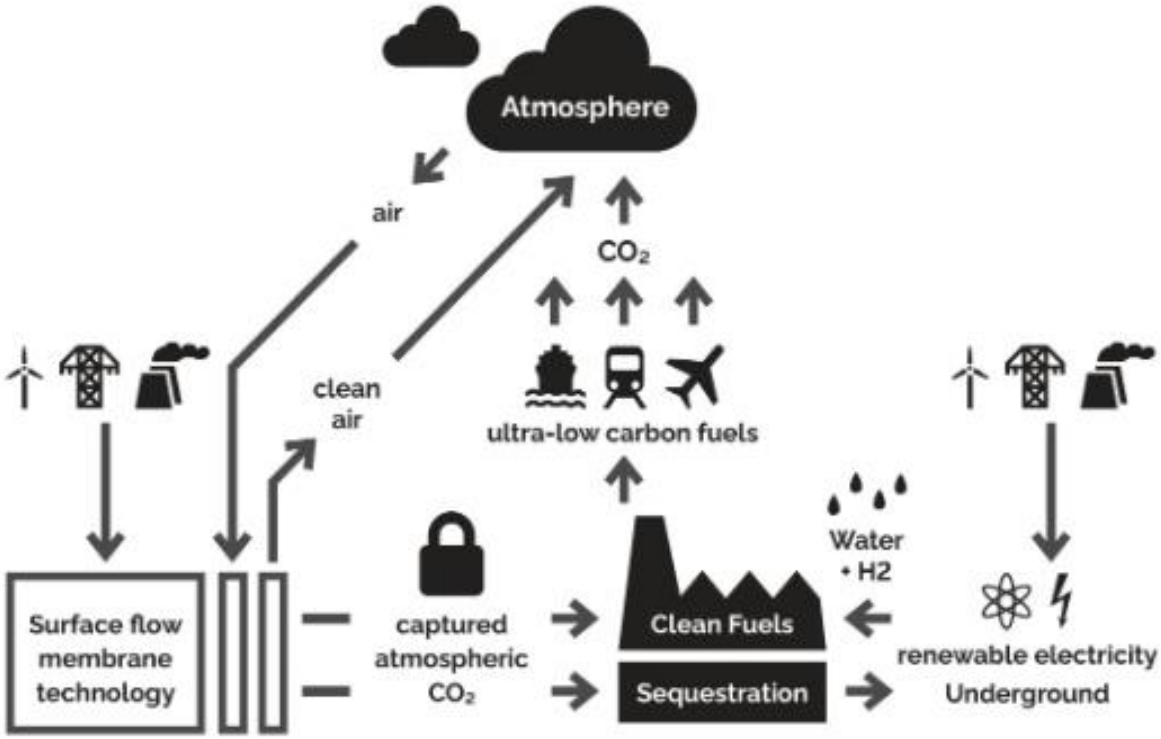

Figure 1. Renewable Energy-driven Membrane Direct Air Capture Technology (Gobina, et al., 2022)

Inorganic Membrane Systems

Inorganic membranes are usually made from metallic oxides, metals, or elementary carbon. They can operate under harsher conditions than their polymeric counterparts and are highly selective and permeable for specific molecules. Inorganic membranes are made as standalone tubes and tubes if they are sufficiently permeable. However, that is not the case, they are made as thin films on multi-layered supporting structures. In porous inorganic membranes, a porous thin top layer is cast onto a porous metal or ceramic support.

Figure 2 show photographs of porous ceramic support (a) and porous metallic support (b). The support provides mechanical strength, and thus offers minimum mass-transfer resistance. Carbon, silicon carbide glass, titania, zeolite membranes, and so on are mainly adopted as porous inorganic membranes supported on different metallic and ceramic substrates, such as α-alumina, γ-alumina, zirconia, porous stainless steel, or zeolite.

Figure 2. Photographs of Tubular Porous Ceramic Membranes (Left) and Tubular Porous Stainless-Steel Membranes (Right)

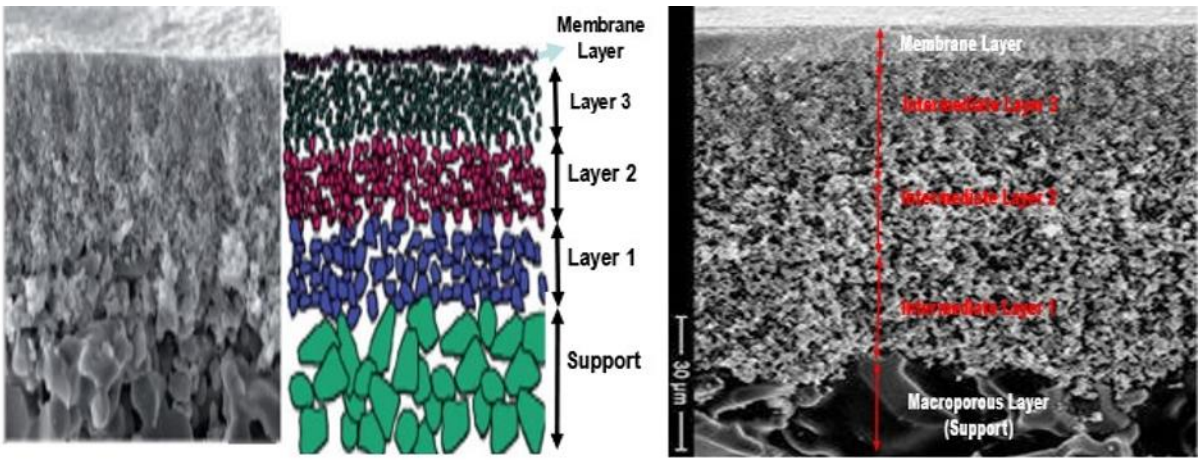

Figure 3. Typical Multi-Layered Asymmetric Ceramic Membrane Structure

Ceramic Porous Support Composition and Manufacture

Ceramic membranes are made up of several different kinds of metal oxides including alumina (Al_2O_3), zirconia (ZrO_2), silica (SiO_2) and titania (TiO_2) (LENNTECH, https://www.lenntech.com/ceramic-membranes-features.htm). The first ceramic membranes globally were produced in France in the 1980s for the purpose of

enriching uranium for the nuclear industry. After several of the nuclear power plants were functioning in France other industrial application areas for these ceramic membranes were found out. Simultaneously, academic research into ceramic membrane systems was being conducted on several fronts such as water treatment, natural gas processing, air separation, hydrogen purification and possible use in reactor systems. A typical commonly reliable process for producing ceramic tubular membrane support is shown in Figure 4.

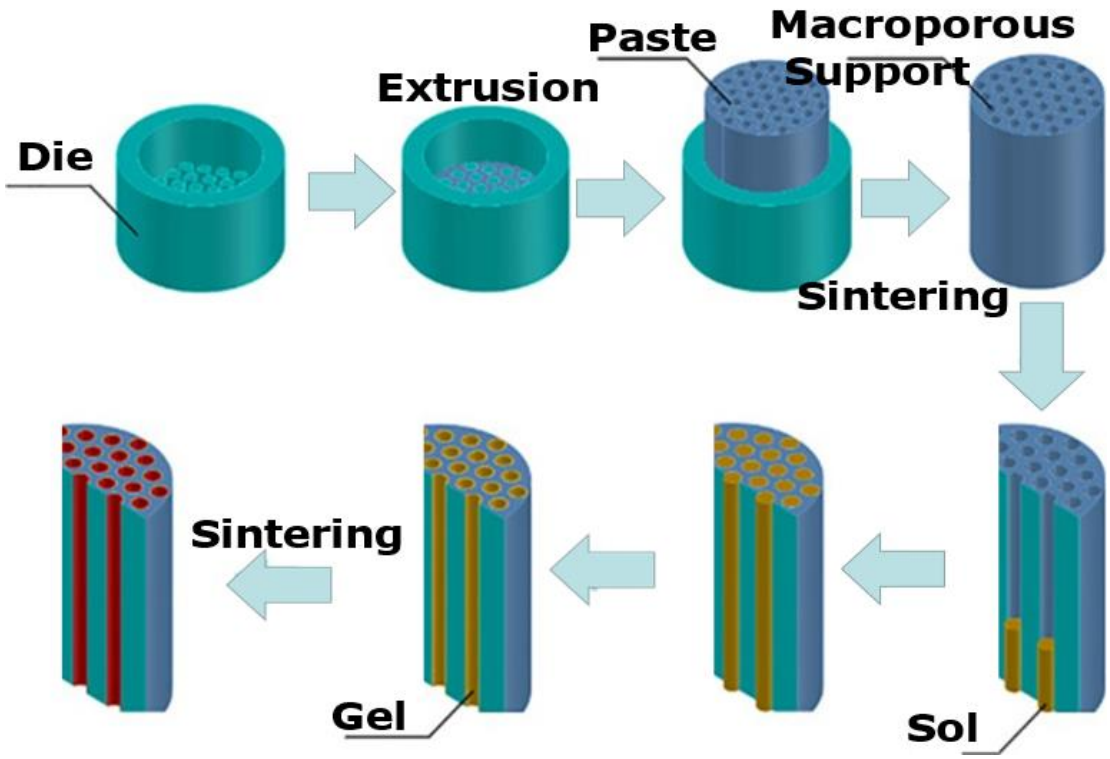

Figure 4. A Schematic Diagram of Production Process for Ceramic Tubular Membrane Supports

The macroporous support is subsequently obtained by extruding a specific paste with a die applied to effect control of the paste shape (such as number of channels, inner and outer diameters). The extrudate is subsequently dried and sintered vertically in a furnace under different controlled heating and cooling regimes.

Metallic Porous Support Composition Manufacture

The other type of support is the porous metal filter. Although several techniques can be potentially used for the fabrication of porous metal membranes, one of the main approaches that has been used for fabrication of unsupported porous metal membranes is particle sintering. Sintering of metallic particles is derived from traditional powder metallurgy technology, whereby hot-compression of micrometre-sized metal particles or fibres at the softening temperature of the metal produces a semi-porous network.

A range of conditions (e.g., particle size, sintering atmosphere) impacts significantly on the quality of the

products from the sintering process and larger particles not only limit neck formation (due to the slow rate of mass transport), but also lead to a mechanically unstable membrane due to the more favourable finger-like macro-voids appearance.

Also, the properties of the metal powders (e.g., size, compressibility, and reactivity) used for sintering must be well characterized to determine the most appropriate heating technique and avoid densification which can occur due to over-heating. The pore size generated using sintering is controlled by the average particle deformation that is induced by the process and the surplus distance between the particles after sintering. Altering the sintering atmosphere during the sintering process can also change the morphology such that sintering most often leads to large pores (e.g., >1 μm).

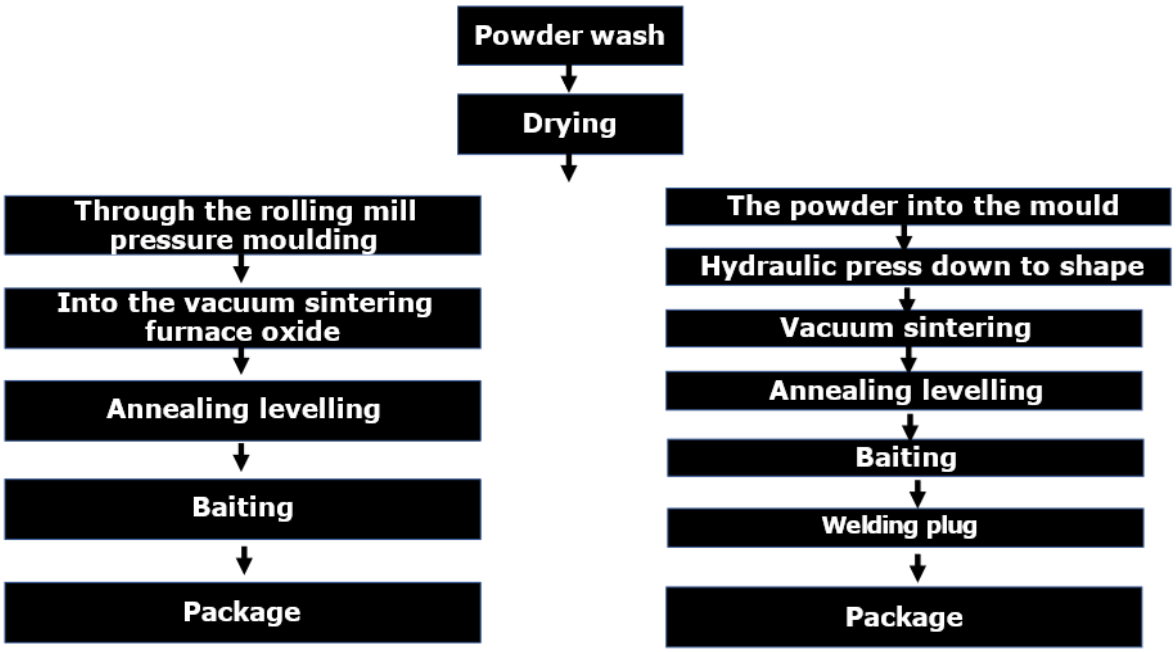

Figure 5. A Schematic Diagram of Production Process for Porous Metallic Tubular Membrane Supports

Preparation of the Thin Separation Layer (Coated Membranes (CMs))

Various methods can be used to fabricate the top membrane layer (thin separation layer) as shown in Figure 6. These include methods such as chemical vapor deposition (CVD), sputtering, and sol-gel processes (Figure 6). Several factors impact the cost of system fabrication; most often, the deposition cost of thin layer membrane materials is dominant. If the deposition process requires high temperatures, it also leads to high process costs. In addition, various limitations caused by the necessity for high temperature and vacuum still exist in depositing top layers. The various deposition processes used for fabrication of top layers are continuously being developed using new methodologies. The various processes can be categorized into three main classes, based on the materials status followed by a detailed classification (see Figure 6).

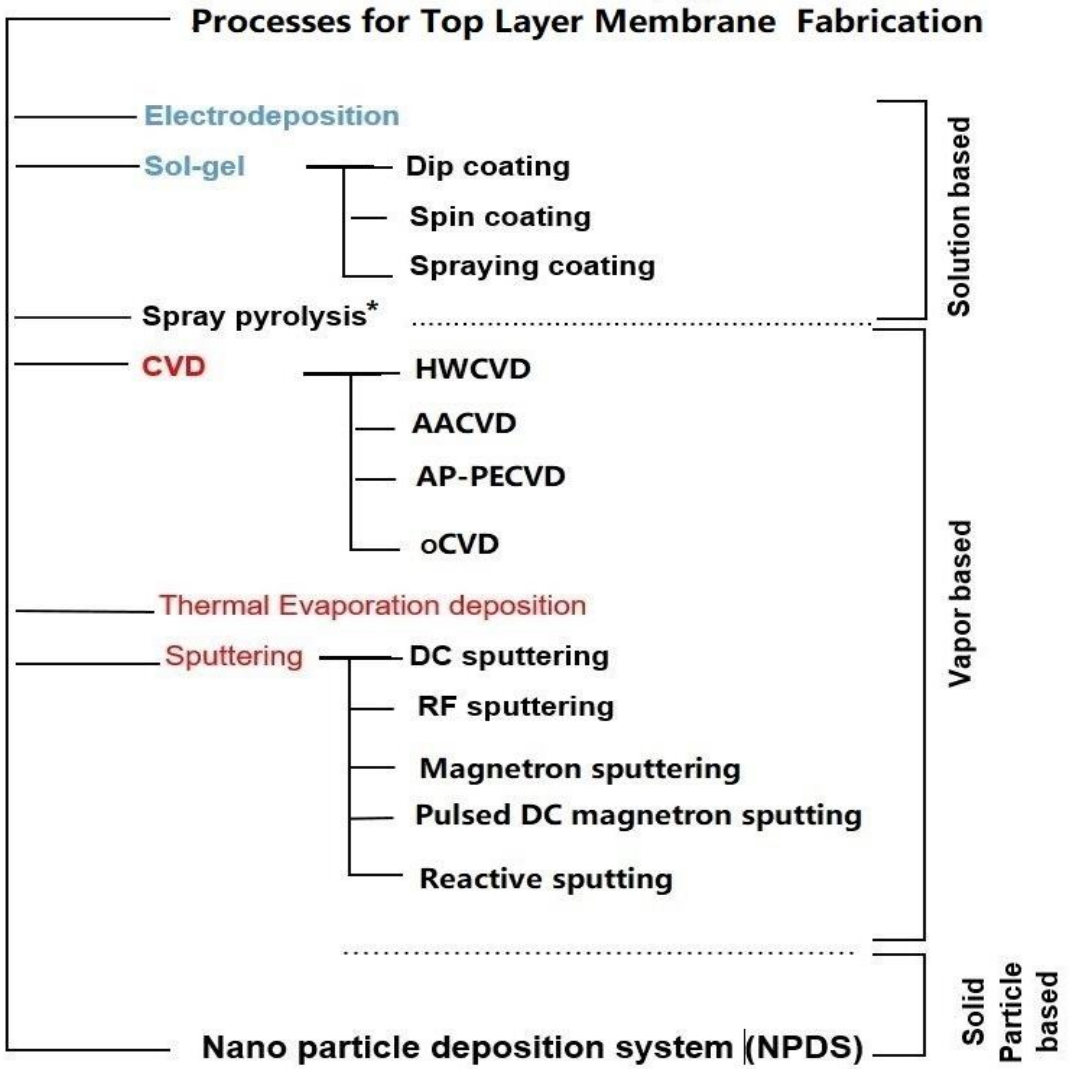

**Spray pyrolysis is in between solution and vapor base*

Figure 6. Fabrication Methods for Membrane Top Layer

Generally, the environment will depend on the deposition technology or relevant status of the precursor. If the processes are based on using solutions, then the main parameter will be the temperature rather than vacuum. However, the vacuum dominates in the vapor-based processes. In electrodeposition and sol-gel processes, which include spin coating, dip coating, and spraying, solution-based processes are well-known. CVD, sputtering, thermal evaporation are processes based on vapours. These vapor-based processes can be classified in a number of ways, such as aerosol-assisted CVD (AACVD), hot-wire CVD (HWCVD), oxidative CVD (o-CVD), magnetron sputtering, pulsed DC magnetron sputtering, atmospheric pressure-plasma enhanced CVD (AP-PECVD), direct current (DC) sputtering, radiofrequency (RF) sputtering and reactive sputtering, depending to their materials and process parameters. Spray pyrolysis can be classified between vapor and solution processes because a solution is normally sprayed but it is deposited as a vapor. Recently, direct material deposition has been tried at room temperature.

Literature Review

Several efforts have been recently devoted to the development of polymeric membrane materials with high CO_2 permeance. In literature, Kolodji, B (2019) has reported the use membranes are to perform direct air capture (DAC) by extracting and mildly concentrating the CO_2 in air from 400 ppm to over 1200 ppm (a factor of 3 or more increase), and sending this concentrate into low pressure ducting destined for a greenhouse. When atmosphere inside the greenhouse is increased to between 600 and 1200 ppm CO_2, a practice known as crop carbon enrichment, the biomass and yield of the crop correspondingly increases.

Yoo et al. For example, reported defect-free Teflon-based membranes having a CO_2 permeance of ~31,500 GPU (GPU: gas permeance unit (1 GPU = 7.5×10^{-12} m^3(STP) m^{-2} s^{-1} Pa^{-1}, STP: standard temperature and pressure) with a CO_2/N_2 selectivity of 3.3 (Yoo MJ, Kim KH, Lee JH, Kim TW, Chung CW, Cho YH, et al., 2018). Free-standing siloxane nanomembranes with high CO_2 permeances exceeding 40,000 GPU have also been reported (Fujikawa S, Ariyoshi M, Selyanchyn R, Kunitake T., 2019). Such membranes with ultrahigh gas permeance would have the potential to capture CO_2 efficiently, even from the air, since the gas permeance resistance through the membranes is quite small, but the CO_2 selectivities are very low and polykers generally degrade even under atmospheric DAC conditions.

With regards to the support Shi, W., Yang, C., Qiu, M., Chen, X., and Fan, Y., (2022) reported on a new method that a γ-Al_2O_3 multilayer ultrafiltration (UF) membrane on an α-alumina (α-Al_2O_3) substrate was successfully fabricated *via* the sol–gel processing method. Zhou S., Xue A., Zhang Y. *et al.*, (2015), designed one-step preparation of high-performance bi-layer α-alumina ultrafiltration membranes supported on coarse tubular substrates by co-sintering process. In their approach, boehmite sol and alumina nanoparticles were mixed in different ratios for the fabrication of microfiltration layer and the ultrafiltration layer. The thickness of the microfiltration layer and the ultrafiltration layer was controlled to be 40–50 μm and about 1 μm, respectively. In their contribution. Yin, X., Guan, K., Gao, P., Peng, C., and Wu, J. (2018) proposed a new method called "precursor film firing method" for improving the permeance of ceramic microfiltration membranes by avoiding intermediate layers and dip-coating process, and efficiently control the thickness of the separation layer. Moreover, Qin, W., Peng, C., Wu, J. (2017) reported on a sacrificial interlayer-based technique used to produce membranes without any intermediate layers in a single-step coating preparation of highly permeable alumina microfiltration membrane on as-prepared alumina supports.

Based on our recent achievements in the membrane field, it is meaningful to evaluate the potential of inorganic membrane for the first time as an alternative DAC process. Two types of inorganic membranes are being developed. A more dense system based on silica and a porous support with an affinity material deposited in the porous network that acts to create an adsoptive selective surface for the flow of CO_2. This article presents experimental results for the silica-based inorganic membrane system for assessing the performance and applicability for DAC from a practical perspective

Materials and Methods

Materials

The supports consisted of aluminium oxide Al_2O_3, 23% titanium oxide TiO_2 and 1% impurity and was supplied by Ceramique Techniques Industriels (CTI), France. The tubes came with non-permeable glazed ends (0.025 m on either ends). The support tube has seven open parallel channels running the full length of the tube (Figure 7) and had a pore size of 15 nm. It was selected because of its added advantages: chemical inertness, high heat resistance and high mechanical strength (Baker 2004). Other physical characteristics of the support are presented in Table 1. Raw materials and chemical reagents used for the deposition of the thin top layer, including isopentane, silicone elastomer and curing agent (Table 2) were all purchased from Sigma Aldrich, UK. During the whole working process, water (>18.2 MΩ) treated by an ultrapure water system (RFU 424TA, Advantec Aquarius, Toyo, Japan) was employed for washing and cleaning.

Figure 7. Ceramic Support: Total Length (left) and Internal Channels (right)

Table 1. Characteristics of the Support

Support Parameter	**Symbol**	**Value**
Total length	L_t	0.366m
Effective length	L_e	0.316m
Outer diameter	D_o	0.0256m
Inner diameter	D_i	0.0206m
Weight of support	W_o	281.3g
Effective permeable area	$A_{eff} = \pi D_o \times L_e$	0.0254m^2
Diameter of each channel	D_{ch}	0.0047m
Number of channels	N_{ch}	7
Pore size of the support	r_p	15nm

Table 2. Chemicals used for Thin Top Layer Membrane Preparation

Component	**Amount**
Isopentane	900 mL
silicone elastomer	100 mL
curing agent	10 mL (or 10%)

Methods

The preparation of the thin film top layer ceramic membrane was carried out using the dip coating method (see Figure 8). Using a precision weighing balance, the initial weight of the unmodified (or uncoated) membrane was measured. Preparation of the modifying solution: 900 ml of isopentane and 100 ml of silicone elastomer base (Sylgard 184) was poured into a beaker. The solution was stirred to attain homogeneity. Thereafter, 10% (or 10 ml) of curing agent (Sylgard 184) was added; and then closed with cellophane to prevent evaporation of isopentane and left for about 20 minutes for occurrence of crosslinking effect (gelation). The solution was then transferred into a measuring cylinder and placed on a magnetic stirrer device. This was done to prevent settling of the elastomer.

(**a**) (**b**)

(**c**) (**d**)

Figure 8. Membrane Modification Process: (a) Support dipped into Solution for Coating, (b) Dried by a Rotating Mechanical Drier under Atmospheric Conditions, (c) Dried in Oven at 65 C and (d) Weighing after Coating.

It is always a good practice to close the cylinder with cellophane to prevent evaporation of isopentane. The support was then submerged or dipped into the solution for 30 minutes. Thereafter, the support was attached to a drying device for 30 minutes to ensure that a uniform distribution of elastomer along the support was achieved. The membrane is then placed and left in an oven for about 2 hours at 65^0 C to evaporate isopentane. These steps

are repeated to achieve the desired gas transport result.

Characterisation

The support and silica-coated membrane were characterised using several methods including liqiud nitrogen adsorption/desorption at 77K. This was carried out using an automated gas sorption analyser (Quantachrome instrument version 3.0) to determine the total surface area and pore size distribution. The isotherms have been described using the Brunauer Emmett and Teller (BET) and the Barrett-Joyner-Halenda (BJH) methods respectively. The surface morphology of the support and membrane was examined using a Zeiss EVO LS10 scanning electron microscopy coupled with the energy dispersive analysis x-ray (SEM/EDAX) to examine the thin top silica layer of the membrane.

Fourier transform infrared coupled with an attenuated total reflection (Nicolet iS10 FTIR-ATR) was used for the structural examination of both the support and silica membranes. The contact angle was measured by the Theta Flex Optical Tensiometer (also known as a goniometer, contact angle meter & drop shape analyser) sessile drop method using a syringe pump to produce the droplet of liquid, and a camera to observe the droplet on a substrate. Software connected to the camera is used to identify and calculate the contact angle of the droplet on the substrate. Theta Flow is a premium instrument for measuring contact angle, surface tension, surface free energy, dynamic contact angle and Static contact angle. Permeation measurement were also applied to determine the gas flow rate through the membranes contained in a shell and tube arrangement in cross-flow mode.

Membrane Gas Transport Mechanisms

CO_2 removal from the atmosphere can be achieved in several ways including water-scrubbing, pressure swing adsorption, cryogenic separation, and membrane separation. Among these, membrane technology stands out as an excellent opportunity regarding simplicity and flexibility, whereas it comprises low energy expenditure for the process associated with low costs. The key issue with membrane-based gas separation processes in general and particularly DAC is that the driving force for the separation (which is the difference in partial pressure of the gas species across a membrane barrier) must be high. In DAC the concentration of CO_2 in the atmosphere is only 421 parts per million means that its partial pressure is only 0.000421 bar. This low pressure means individual gas constituents such as CO_2, O_2, N_2 in air can be separated attending to their different permeability rates through a porous membrane material, or to different solubilities and diffusivities through a nonporous, dense membrane material depending on their properties (see Table 8).

Effective separation takes place when some gas constituents pass through the membrane barrier quicker than others. This process can be described by three general transport mechanisms: Knudsen diffusion, solution-diffusion, or molecular sieving. However, there are generally seven gas transport mechanisms that can occur in

porous and dense membrane systems (Figure 9). The different mechanisms apply when the membrane satisfies specific structural conditions, as shown in Figure 9.

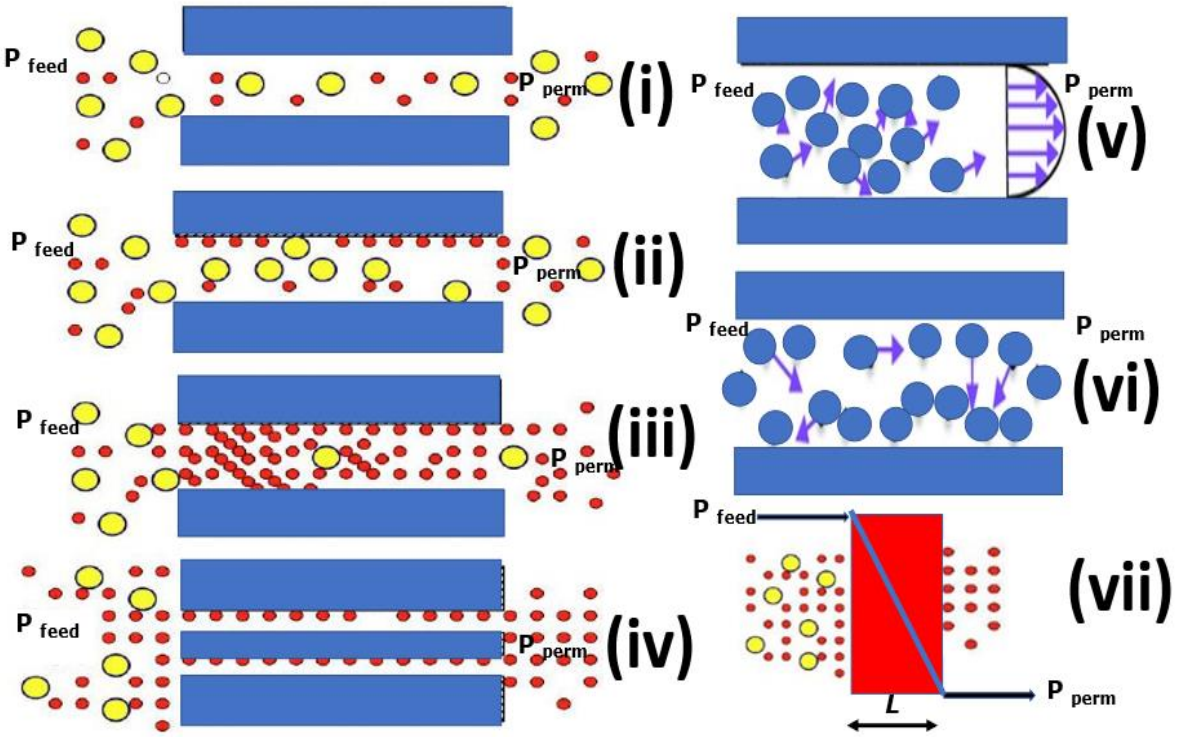

Figure 9. Porous and Dense Membranes Systems and their Gas Permeation Mechanisms. (Microporous and Mesoporous Membrane Gas Transport Mechanisms ((i) Knudsen Diffusion, (ii) Surface Diffusion, (iii) Capillary Condensation, (iv) Molecular Sieving), Macroporous Membrane Gas Transport Mechanisms ((v) Viscous Flow, (vi) Molecular Diffusion) and (vii) Solution Diffusion.

Microporous Membrane

In the case of gas transport through microporous membranes (e.g. silica membranes), there is an Arhenius-type temperature dependence behavior which affects the performance at elevated emperatures. It is well understood that this happens when kinetic diameter of the molecule approaches that of the pore diameter and results in very high perm-selectivity (separation factor)s. This mechanism is known as activated gas transport. It has been found that the phenomenological flux J (mol.m^{-2}. s^{-1}) through microporous materials increases as function of temperature according to Equation 1:

$$J \propto J_0 \exp\left(\frac{-E_{act.}}{RT}\right) \quad (1)$$

Where $E_{act.}$ (KJ.mol^{-1}) is an apparent activation energy. Depending on micropore size and gas molecule size, activation energies ranging from around 2 to 40 KJ.mol^{-1} have been reported (Liguori, S. and Wilcox, J., 2017).

Mesoporous Membranes

In mesoporous materials, as for example γ-alumina membrane, the gas transport mechanisms are: (i) Knudsen diffusion, (ii) laminar (or Poiseuille) flow and (iii) surface diffusion. However, according to these mechanisms, transport rates decrease as function of temperature as shown by Equations 2-4.

Knudsen Diffusion

$$F_{kn,0} = \frac{2.\epsilon_p.\mu_{Kn}.\bar{\upsilon}.\check{r}}{3RTL} \; with \; \bar{\upsilon} = \sqrt{\frac{8RT}{\pi M}} \qquad (2)$$

Where $F_{Kn,0}$ is the Knudsen permeation (mol.m^{-2}. s^{-1}Pa^{-1}), ϵ_p is the porosity (–), μ_{Kn} is a shape factor (–) equal to 1/τ, where τ is the tortuosity, R is the gas constant (J.mol^{-1}. K^{-1}), T is the absolute temperature (K), ř is the modal pore radius (m), $\bar{\upsilon}$ is the average molecular velocity (m.s^{-1}), L is the layer thickness (m) and M is the molecular mass (kg.mol^{-1}) of a gas molecule.

Surface diffusion

$$J_{S.0} = -\rho_{app}.D_S.\mu_s\frac{dq}{dl} \qquad (3)$$

Where $J_{s.0}$ is the surface diffusion flux component (mol.m^{-2}. s^{-1}), P_{app} is the apparent density (kg.m^{-3}), defined as (1- ϵ_p) ρ_{cryst}, D_s is the surface diffusion coefficient (m^2. s^{-1}), μ_s is the reciprocal tortuosity (–) and dq/dl the surface concentration gradient (mol.kg^{-1}. m^{-1}). The activation energy for diffusion is strongly correlated with the heat of adsorption. Since it is assumed that diffusion takes place by molecules which jump from one site to another, the activation energy is a fraction of the heat of adsorption [36]. This implies that: a) strongly adsorbed molecules are less mobile than weakly adsorbed molecules, and b) that the total flux will decrease as the temperature is increased since the increased diffusivity is overruled by the decrease in surface concentration.

Capillary Condensation

$$\frac{\rho RT}{M} \ln\frac{P_t}{P_0} = -\frac{2\sigma\cos\theta}{r} \qquad (4)$$

Where ρ is the density of the condensate (kg/m^3), P_0 the temperature dependent saturation vapour pressure for a planar interface (Pa), σ the interfacial tension(N/m), θ the contact angle and r the radius cylindrical capillary. Multilayer adsorption takes place when a species is adsorbed in several layers and is an extension of monolayer adsorption. Surface diffusion models are usually valid for up to monolayer coverage and can be extended to also include multilayer diffusion. Due to monolayer and subsequent multilayer diffusion, the permeability will

increase until an optimum is reached as capillary condensation begins and a liquid meniscus appears. After this point the permeability usually decreases because of the liquid transport contribution.

Macroporous Membranes

Laminar Flow

$$F_{p,0} = \frac{\varepsilon_p \mu_p}{8RT} \frac{r^2}{\eta L} P_m \quad (5)$$

Where $F_{kn,0}$ is Poiseuille permeation (mol.m^{-2}. s^{-1}. Pa^{-1}), μ_p is the reciprocal tortuosity (–), η is the gas viscosity (N.s.m^{-2}), L is the thickness of the porous layer (m) and P_m is the mean pressure (Pa**). L**aminar flow is also sometimes referred to as viscous or streamline flow**.** Typically, this type of flow occurs at lower velocities, and the fluid flow is characterised by the by the absence of lateral mixing. At low Reynolds number when the viscous forces dominate, they are sufficient to maintain all the fluid particles in line, and then the flow is laminar.

Molecular Diffusion

In the general case, at a constant temperature and pressure, the molar diffusion flux $\dot{n}$ (mol.m^{-2}. s^{-1}) of substance A is directly proportional to dC_A/dyknown as the molar concentration gradient (mol/m³m) and a one – dimensional formulation is described by Fick's law. (Equation (6)).

$$\dot{n}_A = -D_A \frac{dC_A}{dy} \quad (6)$$

Where D_A is the diffusion coefficient (m/s) in a binary system. The flow of one component must be balance by by the counterflow of the other component and therefore

$$\dot{n}_B = -D_B \frac{dC_B}{dy} \quad (7)$$

but since $C_A + C_B$= *const*ant, then

$$\left|\frac{dC_A}{dy}\right| = \left|\frac{dC_A}{dy}\right| \text{ and } D_A = D_B = D_{AB} \quad (8)$$

D_{AB} is known as the interdiffusion coefficient. In order to describe a unidirectional diffusion of molecules A in a multicomponent mixture of ideal gases, the Stefan-Maxwell equation (9) is used

$$\frac{dY_A}{dy} = \sum_{j-A}^{n} \frac{d_A C_j}{C_T^2 D_{A_j}} (u_j - u_A) \quad (9)$$

Equation (9) is based on the kinetic theory of gases, in which Y_A is the mole fraction of component A; C_T is the total concentration (density) of mixture (= p/RT); C_A = pY_A/RT; c_j = pY_j/RT; D_{Aj} is the interdiffusion coefficient for a pair A, j; and u_j and u_A are the rates of diffusion for the components of the pair respectively.

Solution Diffusion Membrane

Gas transport in organic and inorganic membranes can also be governed by the solution-diffusion mechanism. In polymeric membranes permeability is the product of solubility and diffusivity of the permeate specieswithin the polymer matrix while in inorganic metallic membranes the solution-diffusion mechanism occurs especially with hydrogen molecules for example, first dissolving in the metal frame-work at the high-pressure feed side, dissociating into two atoms, atomic hydrogen transporting through the metal membrane thickness and recombining back to the molecular hydrogen at the low-pressure permeate side. The hydrogen flux, *F* (mol.m^{-2}. s^{-1}) across the metal membrane with a thickness *L* (m) can be described by equation (10).

$$F = \frac{P\left(p_{Feed}^{n} - p_{perm}^{n}\right)}{L} \quad \textbf{(10)}$$

Where *P* is the hydrogen permeability (mol. m. m^{-2}. s^{-1}. Pa^{-n}), and p_{feed} and p_{perm} are the hydrogen partial pressures at the high-pressure side (feed) and low-pressure side (permeate), respectively (Pa^n). If the exponent *n* in Equation (10) is equal to 0.5, then Equation (10) represents the well-known Sieverts' law transport mechanism (Sieverts, A. 1929). A deviation Sieverts' law can occur if *n* is different from 0.5 and is an indication of the presence of mass transfer limitations rather than the diffusion in the bulk metal itself.

Results

The results are divided into 3 sections vis; morphology (FTIR-ATR, SEM/EDAX, BET/BJH, contact angle), gas permeation and gas transport characteristics respectively.

Morphology

Results for the morphological characterisation of the support and top thin layer are presented in Figure xxx

through xxx.

Fourier transform infrared spectroscopy (FTIR) with Attenuated total reflectance (FTIR-ATR)

Figure 10 shows FTIR of the support (10a) and that of dip coated silica membrane (10b). From Figure 10a and b, and comparing the FTIR of the support and that of the silica membrane, we can see that the support possed 3 bands on the spectra while the silica coated membrane possed up to 5 bands on the spectra. From Figure 10a, it was discovered that the band at 2335.00 indicated the C – H functional group while the band located at 2167.34 and 1977.73 showed the presence of C – O and functional group. It was proposed that the C – O functional groups could be as a result of the alumina in the original support.

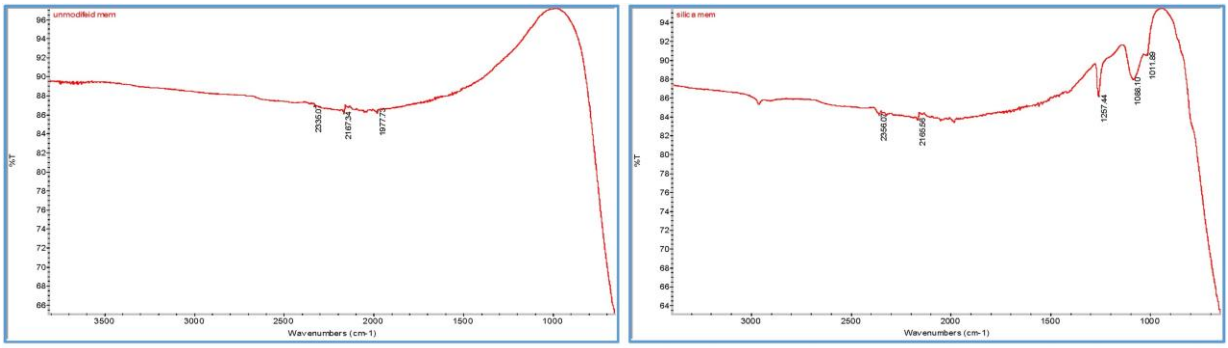

(a) (b)

Figure 10. FTIR-ATR for Support (left) and FTIR forSilica Coated Membrane (right)

From Figurec 10b, it was discovered that the band at 2356.07 designaes the C – H functional group and the bands at 2165.58 and 1257.44 are attributed to the stretching vibrations of C – O and C – O functional groups respectively. In addition the bands at 1088.10 and 1011.89 portray C – O functional group. It was proposed that the C – O and C – O functional groups on the silica membrane spectra might have originated from the silica solution mix that was used for the membrane deposition process.

Scanning Electron Microscopy and Energy Dispersive X-ray analysis (SEM/EDAX)

The SEM/EDAX were carried out to study the surface morphology of the support and the silica membranes. The SEM surface images of both the support and silica coated membrane are presented in Figure 11. Figure 12 shows the EDAX of the support and silica membrane respectively. The support and silica membranes were examine at the magnifications of 100 X and 400 X respectively with the scale of 10μm and 100μm for the silica mnembrane and support respectively. It was observed that the support was constituted of different elemental species including of Al_2O_3 and TiO_2.

However, it observed that SiO_2 was added to the other compounds already present in the support after the dip-

coating process as shown on the EDAX spectra in Figure 12. From the result of the spectra obtained in Figure 132 (left) it can be observed that the support surface exhibted a crack-free plain and clear surface which is an indication that the support was defect-free as confirmed also by the permeation analysis. However, from Figure 12 (right), it was noticed that there were tiny whitish particles on the surface of the coated support which was propounded to have have appeared as a result of silica (SiO_2) adhesion on the support surface (Figure 11-right)

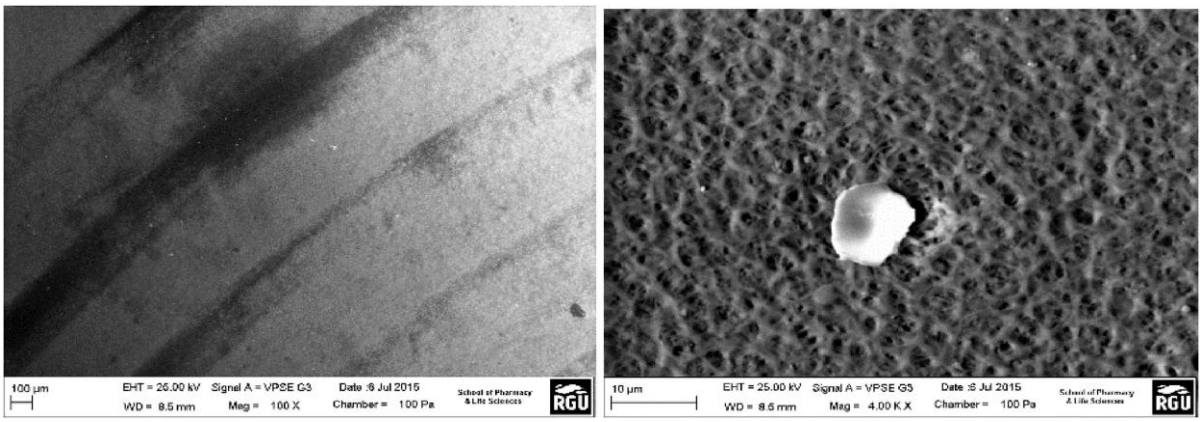

Figure 11. SEM Surface Images of Support (left) and SEM Surface Image of Silica Membrane (right)

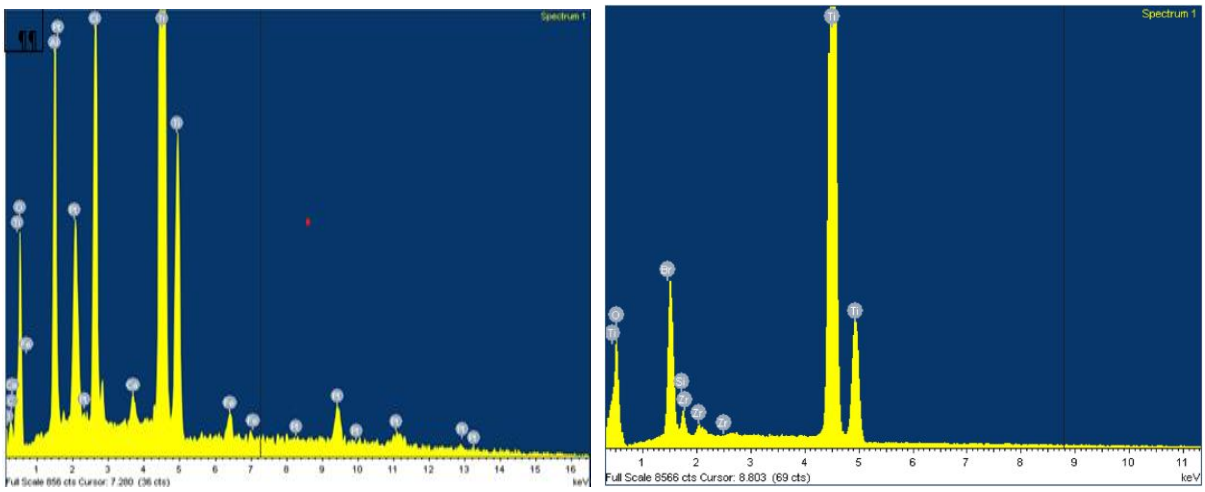

Figure 12. EDAX Spectra of Support (left) and Silica Membrane (right)

Liquid Nitrogen Adsorption (BET and BJH)

Figure 13 depicts the BET surface area whereas Figure 14 shows the BJH pore size of the 1st and 2nd dip-coated silica membrane that were used for the study. From Figure 13 (left) and 13 (right), it was observed that dip-coated membranes posses hysterisis on their curves which suggest that the membrane can undergo a capillary condensation in their mesopores. Figure 14a shows that the hysteresis of the 1st dip-coated membrane was more prominent compared with that of the 2nd dip-coated membrane shown in Figure 13 (right).

From the BJH results of the analysis presented in Figure 14 it is observed that both the 1st and 2nd dip-coated membranes possess a type IV and V isotherm which is in accordance with the mesoporous classification of the membranes. The surface area of the membrane was supposed to witness an increase after each dipping with a reduction in the pore size. The pore size of the silica membrane was analysed using the sum of resistance procedure developed by by Ulhorn and Burgraaf (1991). The pore size of the 1st dip was found to be 3.7 Å while that of the 2nd dip-coated membrane was 3.1 Å. As expected, it confirms that there was a reduction in the pore size of the membrane following the silica modification process as these values compare with the 150 Å of the support.

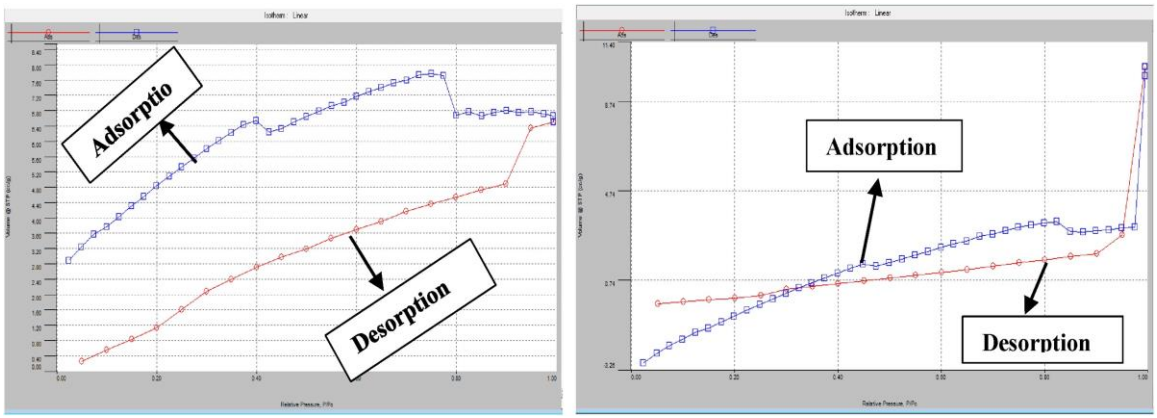

Figure 13. BET Surface Area of Support (left) and Silica Coated Membrane (right)

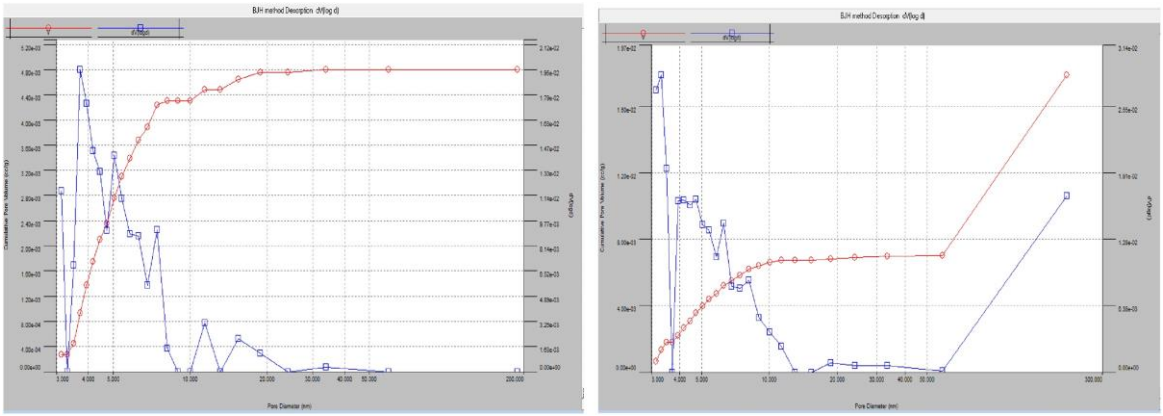

Figure 14. BJH Surface Area of Support (left) and Silica Coated Membrane (right)

Contact Angle and Surface Free Energy or Interfacial Free Energy or Surface Energy

In the scientific community, it is accepted that a surface is described as hydrophobic if its static water contact angle θ is >90º and is termed hydrophilic when θ is <90º. Figure 15 shows the Tensiometer contact angle measurement obtained by dropping model liquids in this case distilled water onto the ceramic support surface (left) NS Silica membrane surface (right). The contact angles formed by a single drop of 5uL distilled water were seen to be for the support (hydrophilic) and for the silica coating (hydrophobic) (see Table 3).

The surface free energy or interfacial free energy or surface energy is a quantitative evaluation of the disruption of the intermolecular bonds that take place in creation of a surface is created. In the physics of solids, surfaces must be intrinsically less energetically favorable than the bulk of a material (the atoms on the surface have more energy compared with the atoms in the bulk of the material), otherwise there would be a driving force for surfaces to be created, removing the bulk of the material. The surface energy may therefore be defined as the excess energy at the surface of a material compared to the bulk, or it is the work required to build an area of a particular surface. Another way to view the surface energy is to relate it to the work required to cut a bulk sample, creating two surfaces. There is "excess energy" as a result of the now-incomplete, unrealized bonding at the two surfaces.

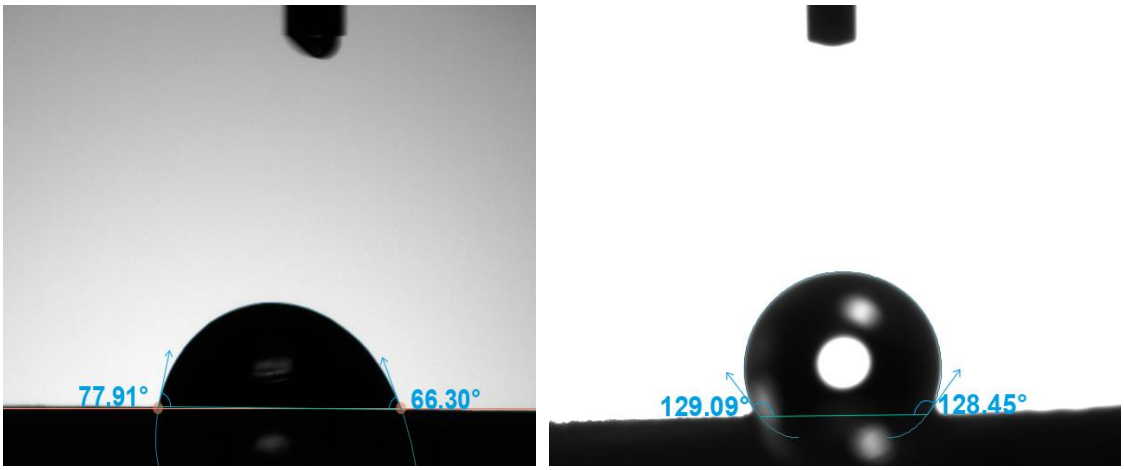

Figure 15. Contact Angle Measurements (0.2 seconds) for the Support (left) and Silica Coated Membrane (right)

Table 3. Experimental Results of Contact Angle for Silica Membrane and Support

Membrane (Pore size)		**Contact Angle [θ]**		**Surface Free Energy (y^{tot} [mN/m]/y^{d} [mN/m])**	
Support	**Silica Coat**	**Support**	**Silica Coat**	**Support**	**Silica Coat**
15nm	3.7nm	76.642	128.77	37.58/37.58	72.80/21.80

Gas Transport Characteristics

Figure 16 shows gas permeation plot versus feed pressures for the three gases considered. Due to its lowest molecular mass methane is observed at higher transmembrane pressure drop to be the most permeable of the three gases (see Figure 16) and shows that permeation rate is inversely proportional to the molecular mass of the gases through the uncoated support.

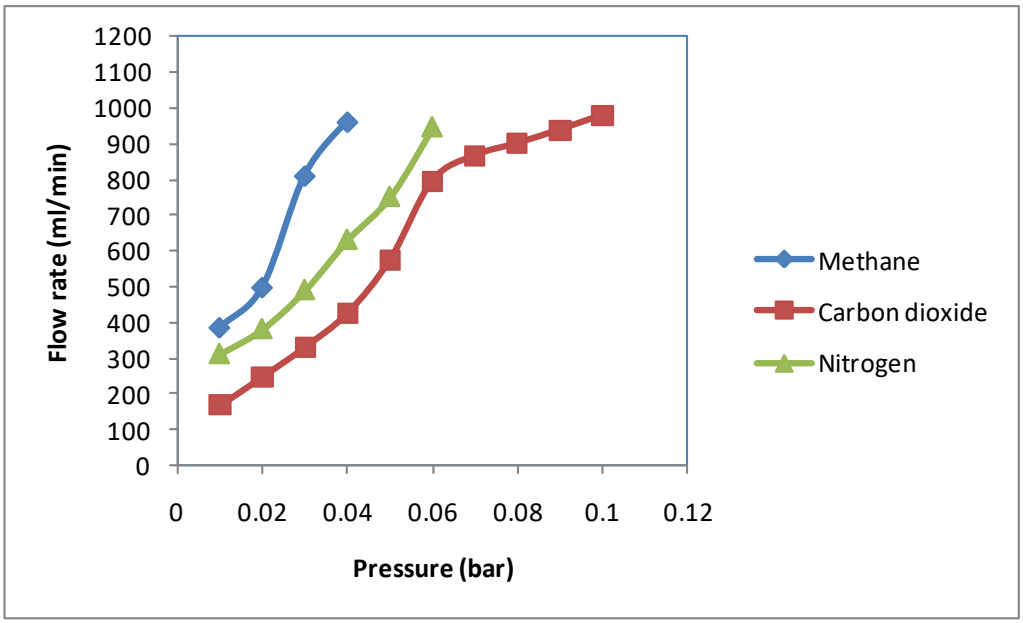

Figure 16. Gas Permeation through Support

Effect of Dip-coating of Thin Top Layer on Permeation Flowrate

As expected, gas permeation flow rates decreased with each modification. The experimental data for CO_2 transport through the support, 1st and 2nd dip is shown in Figure 17. Figure 17 is used to track the changes in flow rates for each coating and at different transmembrane pressure drop for the case of CO_2. Overall, each coating shows an appreciable drop in the flow rate, for instance, from 331 to 6.30 ml/min at 0.03 bars and from 575 to 7.80 ml/min at 0.05 bars, etc. This trend is an indication of severe alteration in permeability. Profiles for the progressive decrease in flow rates values for N_2 and CH_4 at different pressures follow a similar pattern to that of for CO_2.

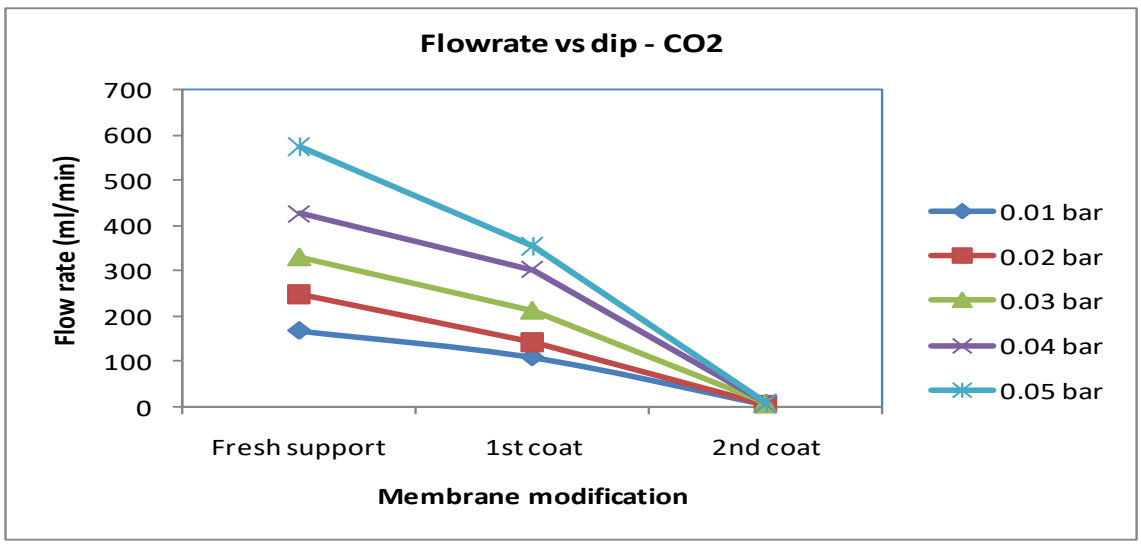

Figure 17. Effect of Number of Thin Top Layer Coating on Flowrate

Effect of Pressure on Flowrate of CO_2 and N_2 through Support and Modified Support

Gas transport results of the experiments conducted are shown in Table 4 for the support, 1st dipping and 2nd dipping respectively at a transmembrane pressure drop of 0.01 to 0.05 bar at room temperature (20° C).

Table 4. Effect of Support Modification on Flow Rate of and N_2

Pressure (bar)	Permeate flowrate (ml/min)					
	Fresh support		1st coating		2nd coating	
	CO_2	N_2	CO_2	N_2	CO_2	N_2
0.01	168	311	109	120	4.49	0.0
0.02	248	381	142	165	5.14	0.0
0.03	331	490	213	233	6.30	0.0
0.04	426	631	303	273	6.75	0.0
0.05	575	751	355	334	7.80	1.07

Experiments were carried out by measurement of crossflow permeation, as described in detail elsewhere (GOBINA, E, US 7048778, 2006). The permeation is defined as the ratio of the transmission flux (quantity of gas crossing a unit area in unit time; in $mol.m^{-2}.s^{-1}$) and the (partial) pressure difference in $mol.m^{-2}.s^{-1}.Pa^{-1}$ (= 1.344×10^{-7} $ml.min^{-1}.cm^{-2}.bar^{-1}$ = 1.93 X $10^{-8}.m^3.m^{-2}.day^{-1}.bar^{-1}$). Gas permeation rates through these membranes are relatively high, mainly due to the very thin top-layers which are in the order of 50-100 nm.

Membrane Perm-selectivity of CO_2 over N_2

The performance of the membrane for separation of a given binary gas mixture of components **CO_2** and **N_2** is typically expressed as follows.

$$\alpha CO_2/N_2 = P_{CO2}/P_{N2} \quad (11)$$

The ratio (P_{CO2}/P_{N2}) is often referred to as the perm-selectivity of the membrane and in the ideal case (ideal gas conditions) it is also referred to as the ideal membrane selectivity. Using equation (5.5) we can calculate values of selectivity as shown in Table 5. CO_2 separation factors are between infinity (∞) and 7.29 over the transmembrane pressure drop of 0.01-0.05 bar. For potential DAC applications, our silica membranes offer unique advantages, such as relatively high selectivity at low pressure drop as summarised in Table 5, and high stability under weathering atmospheric conditions in chemically aggressive atmosphere. As a result, these membranes are considered a viable material for the separation of CO_2 directly from air. Additionally, no liquid or solid consumables are needed once deployed. Indeed, unlike other ceramic membranes, which are affected by the low-temperature phase transition, silica shows reasonable thermal, chemical, and structural stability in both oxidising and reducing environments. Structurally, it can be modified by using different affordable methods and conditions.

Table 5. Membrane Perm Selectivity of CO_2 over N_2

Pressure (bar)	Permeate flowrate (ml/min)		
	Fresh support	1st coating	2nd coating
	Flowrate Ratio ($\alpha CO_2/N_2$)	Flowrate Ratio ($\alpha CO_2/N_2$)	Flowrate Ratio ($\alpha CO_2/N_2$)
0.01	0.54	0.90	∞
0.02	0.65	0.86	∞
0.03	0.68	0.91	∞
0.04	0.67	1.11	∞
0.05	0.77	1.06	7.29

Membrane Separation based on Viscosity

Viscosity is a parameter which plays a major role in determining the rate of Diffusion. Diffusion involves the extension of molecules or atoms from a higher to lower concentration region and viscosity represents the intermolecular friction of a fluid which hinders its motion. Clearly, as Table 6 shows viscous flow mechanism is not in operation in this pressure drop range.

Table 6. Effect of Pressure and Support modification on Flow Rate and Inverse Viscosity Ratio of CO_2 and N_2

Pressure (bar)	Permeate flowrate (ml/min)					
	Fresh support		1st coating		2nd coating	
	Flowrate Ratio (CO_2/N_2)	Inverse Viscosity Ratio $(\eta_{CO_2}/\eta_{N_2})^{-1}$	Flowrate Ratio (CO_2/N_2)	Inverse Viscosity Ratio $(\eta_{CO_2}/\eta_{N_2})^{-1}$	Flowrate Ratio (CO_2/N_2)	Inverse Viscosity Ratio $(\eta_{CO_2}/\eta_{N_2})^{-1}$
0.01	0.54	1.19	0.90	1.19	∞	1.19
0.02	0.65	1.19	0.86	1.19	∞	1.19
0.03	0.68	1.19	0.91	1.19	∞	1.19
0.04	0.67	1.19	1.11	1.19	∞	1.19
0.05	0.77	1.19	1.06	1.19	7.29	1.19

Membrane Separation based on Molecular Weight

Knudsen diffusion is a selective transport mechanism because the diffusion flux is inversely proportional to the square root of the molecular weight of a species. Thus, the mean molecular velocity decreases with an increase in molecular weight. The increase in the flux with increasing temperature is because the concentration of an ideal gas (p/RT) is inversely proportional to temperature. Clearly, as Table 7 shows Knudsen mechanism is not in operation in this pressure drop range.

Table 7. Effect of Pressure and Support Modification on Flow Rate and Square Root of Inverse Molecular Weight Ratio of CO_2 and N_2

Pressure (bar)	Permeate flowrate (ml/min) and Square Root of Inverse Molecular Weight Ratio					
	Fresh support		1st coating		2nd coating	
	Flowrate Ratio (CO_2/N_2)	Square Root of Inverse Molecular Weight Ratio $(MWCO_2/MWN_2)^{-0.5}$	Flowrate Ratio (CO_2/N_2)	Square Root of Inverse Molecular Weight Ratio $(MWCO_2/MWN_2)^{-0.5}$	Flowrate Ratio (CO_2/N_2)	Square Root of Inverse Molecular Weight Ratio $(MWCO_2/MWN_2)^{-0.5}$
0.01	0.54	0.80	0.90	0.80	∞	0.80
0.02	0.65	0.80	0.86	0.80	∞	0.80
0.03	0.68	0.80	0.91	0.80	∞	0.80
0.04	0.67	0.80	1.11	0.80	∞	0.80
0.05	0.77	0.80	1.06	0.80	7.29	0.80

CO_2 Separation Based on Adsorption, Surface Flow, and Kinetic Diameter

Microporous silica membranes can sometimes mimic transport properties of zeolites and carbon molecular sieves which selectively separate molecules based on pore size and polarity and are thus highly tuneable to specific gas separation processes. As shown in Table 8 CO_2 is highly polarised than N_2 and has a smaller kinetic diameter (3.3 Å), compared with (3.64 Å). It is also strongly adsorbed on silica than N_2 and less viscous (15 μPa.s) compared to 17.9 μPa.s for N_2. Table 8 also shows that CO_2 has a smaller kinetic diameter which facilities its transport through available free volume and diffusion pathways in the silica matrix.

Table 8. Gas Properties used to help explain the High CO_2 Perm-selectivity over N_2

Gas	Molecular mass (g/mol)	Kinetic diameter (Å)	Viscosity, @1 atm, 300 K (μPa.s)	Density (kg/m^3)	Critical Temperature (°C)	Critical Pressure (bar)	Condensability (K)	Polarizability (Å)
CO_2	44.01	3.30	15.0	1.842[1)] 1.977[2)]	31.2	35.0	195.0	1.9
CH_4	16.04	3.80	11.1	0.7 – 0.9[2)]	-82.6	46.5	149.0	2.6
N_2	28.01	3.64	17.9	1.165[1)] 1.2506[2)]	-147.0	34.0	71.0	1.4
Air	28.96	---	18.6	1.205[1)] 1.293[2)]	-140.5	37.9	---	---

[1)]NTP – Normal Temperature and Pressure - is defined as *20°C (293.15 K, 68°F)* and *1 atm (101.325 kN/m^2 = 101.325 kPa = 14.7 psia = 0 psig, 30 in Hg = 760 torr)*

[2)] STP - Standard Temperature and Pressure - is defined as *0°C (273.15 K, 32°F)* and *1 atm (101.325 kN/m^2 = 101.325 kPa = 14.7 psia = 0 psig, 30 in Hg = 760 torr)*

CO_2 with higher critical temperature shows the higher condensability which facilitates gas solubility in silica. Higher permeability of CH_4 in comparison to N_2 beside its larger kinetic diameter can be attributed to the higher condensability of CH_4. In general, smaller molecules (small kinetic diameter) and those with stronger

membrane-adsorption properties are adsorbed onto membranes resulting in larger selectivity. The capacity to discriminate based on both molecular size (kinetic diameter) and adsorption affinity makes microporous silica an attractive candidate for CO_2 separation from N_2 and CH_4.

Depending on the nature of the silica selected as the sorbent it can possess small cages of (~5.1×5.1 Å) that are accessible through smaller apertures of (~3.5×3.5Å). Such aperture size is comparable with the kinetic diameters of CO_2 (3.30 Å), CH_4 (3.80 Å) and N_2 (3.64 Å). This suggests the possibility of kinetic separation of the CO_2/N_2 mixture in the atmosphere by exploiting the diffusion rate difference of CO_2 and N_2 through the micro-channels of silica. However, another important mechanism is in operation responsible for excluding N_2 and that is adsorption.

Permeation Models of CO_2 and N_2 in the Silica Micropores

The coated silica membrane shows that permeation is rates reduce with increasing number of dips especially after the second dip. Figure 18 displays the postulated transport of CO_2 and N_2 through silica micropores. Figure 18 schematically describes a typical micropore that shows gas permeation through the silica membrane mimicking a Y-type zeolite (CO_2 molecules are adsorbed on the membrane surface and then migrate into the pores by surface diffusion).

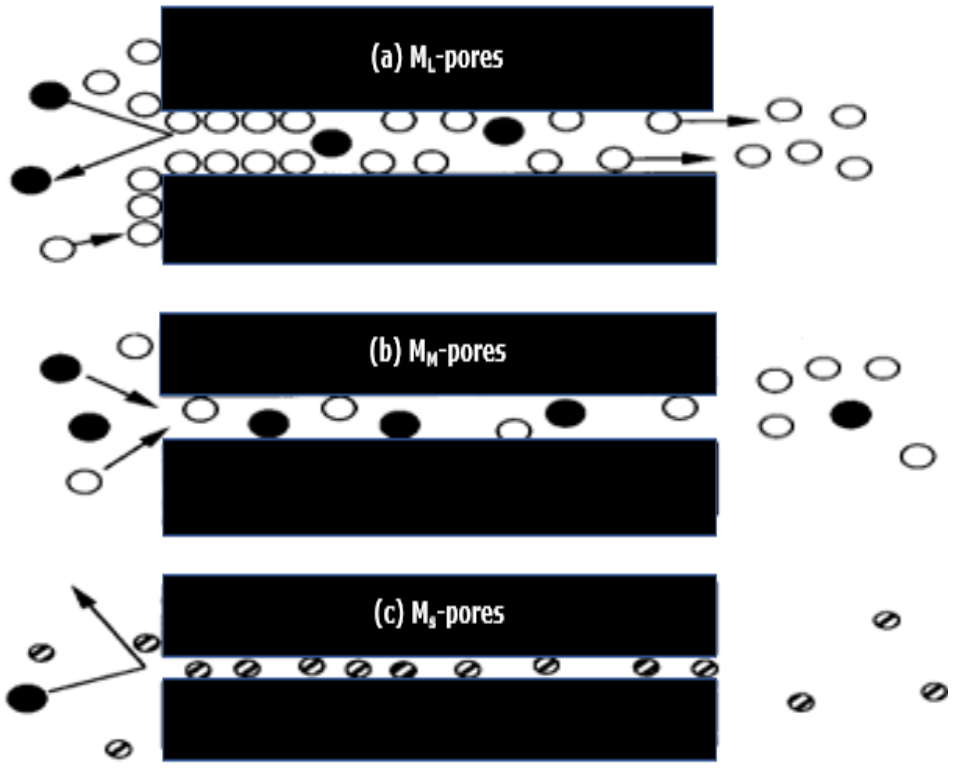

Figure 18. Permeation Models in Micropores; (a) M_L-pores, (b) M_M-pores and (c) M_S-pores (○ -CO_2; ● -N_2 and ⊘ -He or H_2)

Adsorbed CO_2 molecules restrict the openings of micropores and prevent non-adsorptive N_2 from accessing the pores by a translation--collision mechanism. When pressure is increased permeances N_2 were increased but CO_2/N_2 perm-selectivity remained at a high level. This type of membrane possesses crystalline pores of order of 0.74 nm, which permits the permeation described above. These micropores are referred to as M_L-pores (large pores). For the case of M_M pores as pressure is increased above 0.04 bar, N_2 is forced through M_M crystalline pores and cracks. In M_S pores only helium (He) and hydrogen (H_2) can permeate through Ms-pores (small pores), which are the most abundant and are impermeable to CO_2 and larger gas molecules. CO_2 and N_2 permeate through pores in which CO_2 and N_2 are barely able to pass one another (referred to as M_M-pores). Pores which belong to Knudsen diffusion regime (K-pores) are extremely scarce in this membrane. In this case, the diffusion rate is determined by the slowest permeating component, N_2 through M_M-pores. The separation in silica membranes is therefore thought to be controlled by the diffusion in the porous structure of the silica and by adsorption–desorption phenomena. Attenuated total reflectance Fourier transform infrared (ATR/FTIR) spectroscopy on both the support and silica-coated support.

Discussion

The capture of carbon dioxide (CO_2) directly from air (DAC) has attracted significant interest in recent times. The National Oceanic and Atmospheric Administration (NOAA) have calculated its long-time CO_2 concentration at its atmospheric monitoring station, Mauna Loa, Hawaii, averaging 421 parts per million (ppm) for the month of May 2022 which is when the CO_2 gas hits its yearly high (NOAA, 2022).

Comparison of Membrane and Conventional DAC Systems

Figure 19 compares the membrane DAC approach with the traditional processes currently being used. Therefore, chemical reactions with sorbents used in traditional DAC are very slow at these CO_2 concentrations and there is also the difficulty of getting the adsorbed CO_2 out again in a more sustainable capture-and-desorption cycles, which can be very energy intensive. Even leading efforts to build traditional DAC plants, such as those using potassium hydroxide (KOH), sodium hydroxide (NaOH) and calcium hydroxide ($Ca(OH)_2$) suffer serious efficiency issues and incur huge recovery costs, making the hunt for new DAC processes notably urgent.

Despite these drawbacks progress is being made on these traditional DAC systems (despite these drawbacks more effort is current being exacted in simplifying these traditional DAC system process to make it more efficient). Swiss climate tech company Climeworks announced on 28 June 2022 that it has broken ground on its biggest new DAC plant yet named Mammoth, with the capacity to capture up to 4,000 tons of CO_2 per year, for storage in basalt formations. More recently a U.S. climate tech company CarbonCapture Inc. in an exclusive partnership with premier carbon storage company Frontier Carbon Solutions announced on September 16, 2022, that it has plans to build the world's largest carbon capture facility in Wyoming, U.S., called Project Bison

which will capture 5,000 tons of CO_2 per year.

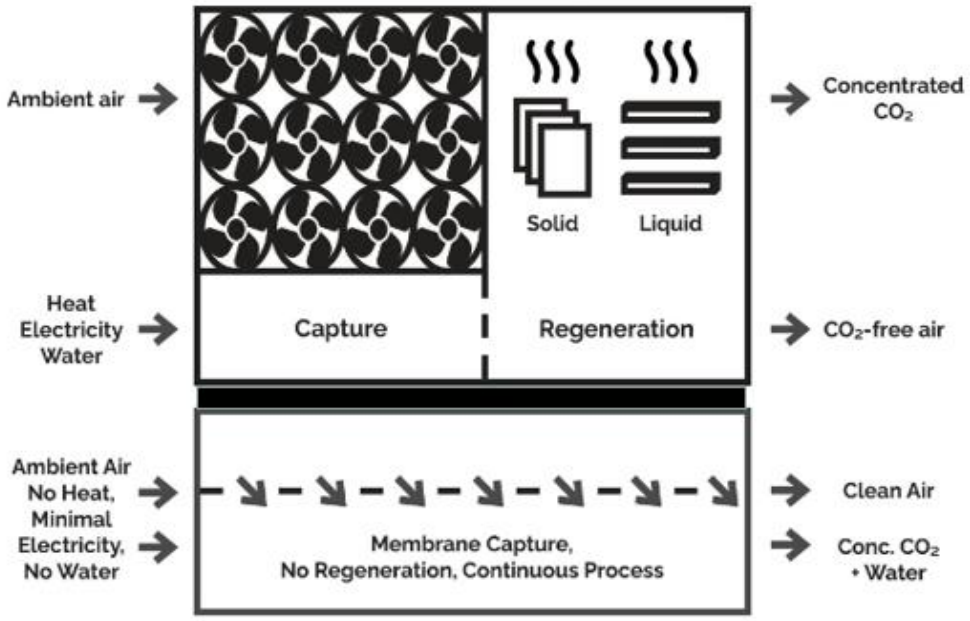

Figure 19. Comparison of Membrane and Conventional DAC Systems (Gobina et al., 2022)

DAC Membrane System Integration with Renewable Energy and CO_2 Utilisation

In this research technical approaches to capture CO_2 from ambient air involving the use of a filter with a transport mechanism as described in previous section have been presented. In practice, moving the air through the filter requires energy as well. For example, to generate sufficient CO_2 partial pressures say 0.02 bar in the air feed, the air must be compressed to 50 bars so that 50x0.000421 = 0.02195 bar and if we are to get a CO_2 partial pressure of 0.04 bar the feed air must be compressed to 100 bars so that 0.000421x100 = 0.0421 bar. Therefore, although our filters need only a tiny transmembrane pressure drop (0.01-0.04 bar) to produce pure CO_2 the feed air needs high total feed pressure of between 25-100 bars to generate the required CO_2 partial pressure. One option is to force the air through the membrane using large fans as is currently being done with adsorbents and solution-based DAC systems. In our silica-alumina composite membrane filters, fans/blowers cannot generate the required pressures of 50-100 bars. Due to this we can capture CO_2 from ambient air by using a compressor to bring the air to 50-100 bars. The use of large fans to push air through the filters as shown in Figure 20 can be used in adsorptive surface flow porous membrane systems that we are currently developing at the Centre. Since the transmembrane pressure drop is low, these porous membrane systems can be integrated with intermittent or variable renewable energy using power electronics-based inverters that convert DC electricity to grid-compatible AC power to then power fans/blowers. The increasing availability of low-cost variable renewable energy (VRE), the deployment of distributed energy resources, advances in digitalisation and growing opportunities for electrification will drive the increasing prominence of VRE and is among the most important drivers of power system transformation globally. The properties of VRE interact with the broader power system, giving rise to several relevant system integration challenges. These challenges do not appear abruptly, but rather

increase over time along with the increase in VRE penetration. With these systems it is possible to create redundancy in the system by calibrating power intensity with power requirements such that at full power all the membrane units are working and at low power one membrane unit is functional.

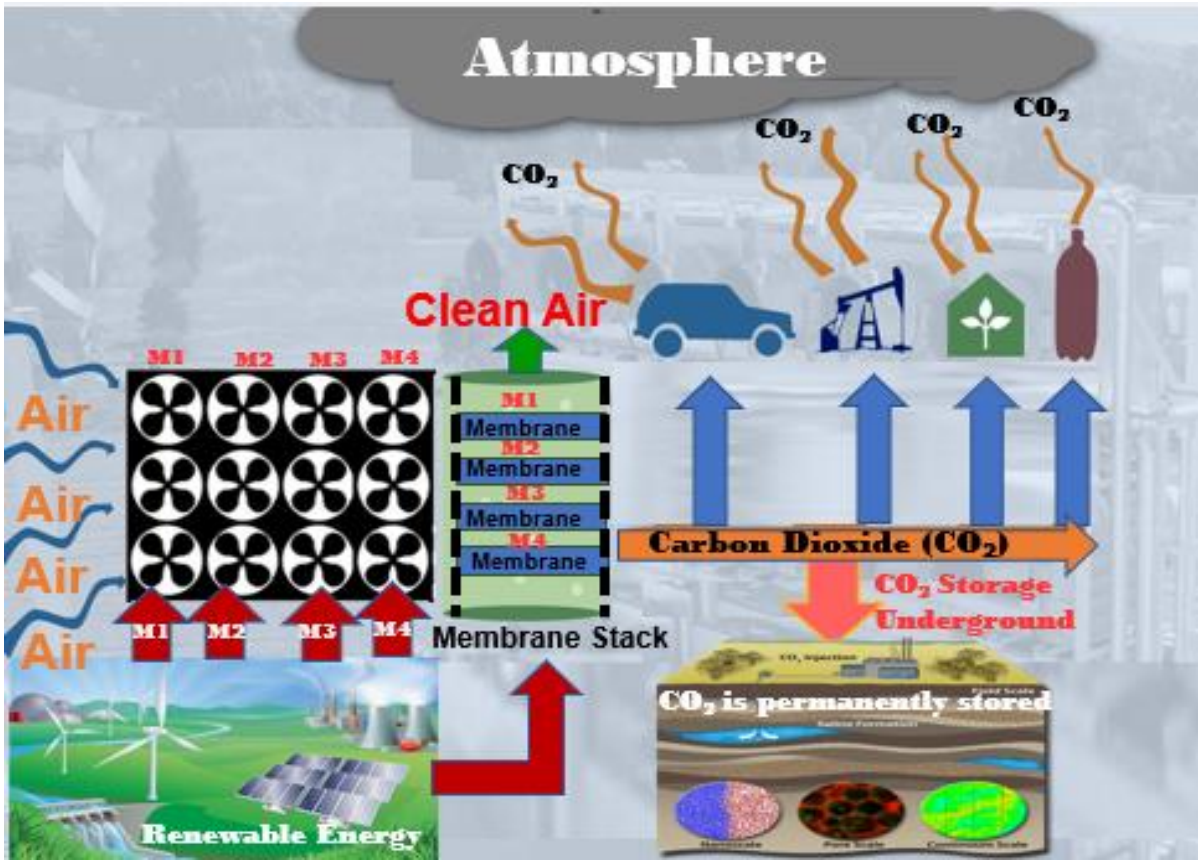

Figure 20. Direct Air Capture Porous Membrane Integration with Renewable Energy and Utilisation

Conclusions and Further Work

This work is the first of its kind to present a membrane approach with repeatable experimental data on the possibility of DAC. Thıs has been achieved through a careful selection of a combination of 15 nm pore support and 2 sequential dip coatings of silica elastomer sol leading to the creation of composite silica membrane that has one of the highest CO_2 perm-selectivity reported in literature. This compares with that reported to date for silica membranes of 300 (Tsai, T., Tam, S-Y., Lu, Y., Brinker, C.J., 2000). In explaining the high CO_2 perm-selectivity shown in our 2nd dip-coated membrane in this study, we have found that it is a combination of adsorption and surface diffusion; and these processes are pressure sensitive such that at pressures between 0.01-0.04 bar, adsorption and surface diffusion are controlling CO_2 flow. However, as pressure is increased above 0.04 bar, any trapped N_2 inside the pores undergo laminar flow and begin to permeate the membrane. The membranes were used to study the permeation of CO_2 and N_2 single gases at room temperature and calculate the perm-selectivity CO_2 of over N_2 based on the ratio of flowrates, viscosity, molecular weight, and kinetic

diameters respectively. It was found that only two successive dip coatings were sufficient to completely block N_2 permeation through the membrane between 0.01-0.04 bar transmembrane pressure drop. Under these conditions only CO_2 permeates the membrane. This is significant in view of the low concentration of CO_2 in ambient air (~421 ppm). The significance of such a prospect means that if porous membrane systems currently being developed by this group become successful, renewable energy can be integrated with CO_2 porous membrane capture system to further reduce legacy carbon and eliminate carbon footprint of the capture process itself. Work is currently being carried out to optimise the pore-modification method, undertake ambient air stream experiments and model the gas transport mechanism.

Acknowledgments

This work is financially supported by matched funding from the Net Zero Technology Centre (NZTC), Scotland, UK and McAlpha, Inc., Calgary, CANADA.

References

Fujikawa S, Ariyoshi M, Selyanchyn R, Kunitake T. (2019), Ultra-fast, selective CO_2 permeation by free-standing siloxane nanomembranes. Chem Lett., 48, 1351–1354. https://doi.org/10.1246/cl.190558

Gobina, E. (2006) A Membrane Apparatus and Method for separating gases, United States of America Granted Patent No. US 7048778, 23-May-2006, https://patents.justia.com/inventor/edward-gobina

Gobina, E., Giwa, A., and Ben-Aron, A. (2022) Unconventional membranes for direct air carbon capture. Membrane technology [online], 2022(7). https://doi.org/10.12968/S0958-2118(22)70077-8

Kolodji, B. (Monday, April 1, 2019 - 1:30pm-1:52pm) Direct Air Capture with Membranes for Crop Carbon Enrichment Proceedings of the AIChE Spring Meeting and Global Congress on Process Safety, 20A, https://www.aiche.org/conferences/aiche-spring-meeting-and-global-congress-on-process-safety/2019/proceeding/paper/20a-direct-air-capture-membranes-crop-carbon-enrichment).

LENNTECH, https://www.lenntech.com/ceramic-membranes-features.htm).

Liguori, S. and Wilcox, J. (2017) Chapter 11 - Silica Membranes Application for Carbon Dioxide Separation,

Editor(s): Angelo Basile, Kmran Ghasemzadeh, Current Trends and Future Developments on (Bio-) Membrane Elsevier, 265-294, https://doi.org/10.1016/B978-0-444-63866-3.00011-X.

NOAA, (June 3, 2022) Carbon dioxide now more than 50% higher than pre-industrial levels, https://www.noaa.gov/news-release/carbon-dioxide-now-more-than-50-higher-than-pre-industrial-levels#:~:text=Carbon%20dioxide%20measured%20at%20NOAA%E2%80%99s%20Mauna%20Loa%20Atmospheric,the%20University%20of%20California%20San%20Diego%20announced%20today

Qin, W., Peng, C., Wu, J. (art A, 2017) PA sacrificial-interlayer technique for single-step coating preparation of highly permeable alumina membrane, Ceramics International, 43(1) 901-904, https://doi.org/10.1016/j.ceramint.2016.09.206].

Shi, W., Yang, C., Qiu, M., Chen, X., and Fan, Y. (2022). A new method for preparing α-alumina ultrafiltration

membrane at low sintering temperature, Journal of Membrane Science, 642, 119992. https://doi.org/10.1016/j.memsci.2021.119992.

Sieverts, A. (1929) The Absorption of Gases by Metals, Zeitschrift für Metallkunde, 21, 37–46, https://www.sciencedirect.com/topics/engineering/sieverts-law

Tsai, T., Tam, S-Y., Lu, Y., Brinker, C.J. (2000) Dual-layer asymmetric microporous silica membranes, Journal of Membrane Science, 169(2) 255-268, https://doi.org/10.1016/S0376-7388(99)00343-9).

Ulhorn, R.J.R. and Burgraaf, A.J. (1991) Gas separatios with inorganic membranes, in Inorganic Membranes: Synthesis, Characteristics and Applications, edited by R.R. Bhave (Van Nostrand Reinhold, New York, 1991), pp. 155–176

Watson, S. K. (June 7, 2022) There's more carbon dioxide in the air than ever before in human history, Popular Science. https://www.popsci.com/environment/co2-emissions-highest-history/#:~:text=Before%20the%20Industrial%20Revolution%2C%20carbon%20dioxide%20levels%20sat,ppm%2C%20which%20was%20first%20breached%20in%20May%201986./

Yin, X., Guan, K., Gao, P., Peng, C., and Wu, J. (2018) A preparation method for the highly permeable ceramic microfiltration membrane – precursor film firing method, *RSC Adv.*, *8*(8) 2906–2914, DOI: 10.1039/c7ra12314k.

Yoo MJ, Kim KH, Lee JH, Kim TW, Chung CW, Cho YH, et al. (2018) Ultrathin gutter layer for high-performance thin-film composite membranes for CO_2 separation. *J Memb Sci.*, *566*, 336–345. DOI: https://doi.org/10.1016/j.memsci.2018.09.017

Zhou S., Xue A., Zhang Y. *et al.*, (2015) Preparation of a new ceramic microfiltration membrane with a separation layer of attapulgite nanofibers. *Mater. Lett.*, 143, 27–30. DOI: 10.1016/j.matlet.2014.12.068.